JOURNAL OF COMPUTATIONAL PHYSICS 61, 64–88 (1985)

A Spectral Collocation Method for the Navier–Stokes Equations

M. R. MALIK*

High Technology Corporation, P.O. Box 7262, Hampton, Virginia 23666

T. A. ZANG

NASA *Langley Research Center, Hampton, Virginia 23665*

AND

M. Y. HUSSAINI†

Institute for Computer Applications in Science and Engineering,
NASA *Langley Research Center, Hampton, Virginia 23665*

Received March 19, 1984; revised December 5, 1984

A Fourier–Chebyshev spectral method for the incompressible Navier–Stokes equations is described. It is applicable to a variety of problems including some with fluid properties which vary strongly both in the normal direction and in time. In this fully spectral algorithm, a preconditioned iterative technique is used for solving the implicit equations arising from semi-implicit treatment of pressure, mean advection, and vertical diffusion terms. The algorithm is tested by applying it to hydrodynamic stability problems in channel flow and in external boundary layers with both constant and variable viscosity.

1. INTRODUCTION

Fourier–Chebyshev spectral methods have been employed in a number of numerical simulations of stability and transition in 3-dimensional wall-bounded shear flows. Specific algorithms have been developed for straight channels [1, 2, 3], curved channels [4], the parallel boundary layer [5], cylindrical Couette flow [6], and pipe flow [5]. In all of these methods Chebyshev expansions are employed in the direction normal to the walls and Fourier methods are used in the remaining

* Research was supported for the first author by the National Aeronautics and Space Administration under NASA Contract NAS1-16916 while employed at High Technology Corporation, P. O. Box 7262, Hampton, Va. 23666.

† Research was supported for the third author by the National Aeronautics and Space Administration under NASA Contracts NAS1-15810, NAS1-16394, NAS1-17070, and NAS1-17130 while in residence at ICASE, NASA Langley Research Center, Hampton, Va. 23665.

0021-9991/85 $3.00

two directions. Hence these methods are applicable whenever periodic boundary conditions are appropriate in two directions.

These methods usually handle the pressure and vertical diffusion terms implicitly, the pressure term so that the incompressibility condition is enforced and the vertical diffusion term in order to relax the diffusive time-step limitation. (The only exception is the method [4] which eliminates the pressure by a clever choice of divergence-free velocity expansion functions.) Algorithms which employ time-splitting [1, 5] can achieve a relaxation of the advective time-step limit by a semi-implicit treatment of the streamwise advection. These implicit equations are solved by a direct method for which the efficiency depends upon simple mean velocity profiles and constant viscosity. However, there are situations in which time-splitting errors are a serious problem [6].

If the spectral discretization in the normal direction is replaced with a finite difference method, then the direct solution of the implicit equations can be performed efficiently for mean flow profiles and viscosities with an arbitrary dependence upon both the normal coordinate and time. Such Fourier-finite difference codes have been utilized both for channel flow [7] and for the parallel boundary layer [8]. The price for this extra flexibility, however, is greatly reduced accuracy in the normal direction.

The contribution of the present paper is the description of a Fourier–Chebyshev algorithm for wall-bounded shear flows which combines the accuracy and efficiency of a fully spectral scheme with the flexibility of a Fourier-finite difference method. The key feature of this algorithm is a preconditioned iterative technique for solving the implicit equations arising from the semi-implicit treatment of the pressure, mean flow, and vertical diffusion terms. This algorithm is applicable to most of the cases described above—channel flow, parallel boundary layers, curved channel flow, and cylindrical Couette flow. Relatively minor modifications are required to treat the different cases. Illustrations will be provided here for straight channel flow and for parallel boundary layer flow with constant and variable viscosity. The discussion will be restricted to 2-dimensional flow. The addition of a second periodic direction is straightforward.

2. Discretized Navier-Stokes Equations for Channel Flow

The rotation form of the 2-dimensional incompressible Navier–Stokes equations is

$$u_t - v(v_x - u_y) + P_x = (\mu u_x)_x + (\mu u_y)_y \tag{2.1}$$

$$v_t + u(v_x - u_y) + P_y = (\mu v_x)_x + (\mu v_y)_y \tag{2.2}$$

$$u_x + v_y = 0, \tag{2.3}$$

where the variable P denotes the total pressure and subscripts denote partial derivatives. The viscosity μ is presumed to depend upon y and t only and the density is taken to be unity. Periodic boundary conditions in x and no-slip boundary conditions at $y = \pm 1$ are assumed.

The spatial discretization of Eq. (2.1)–(2.3) employs spectral collocation. The collocation points are

$$x_j = jL_x/K \qquad j = 0, 1, \ldots, K-1, \tag{2.4}$$

$$y_m = \cos\left(\frac{m\pi}{N}\right) \qquad m = 0, 1, \ldots, N, \tag{2.5}$$

where L_x is the periodicity length in the streamwise direction, and K and N are the number of intervals in the x and y directions, respectively. The dependent variables have Fourier–Chebyshev series of the form

$$u(x, y, t) = \sum_{k=-K/2}^{K/2-1} \sum_{n=0}^{N} u_{kn}(t)\, e^{2\pi i k x/L_x} T_n(y), \tag{2.6}$$

where T_n is the Chebyshev polynomial of degree n. In the spectral collocation method, spatial derivatives of u are obtained by differentiating the series expansion coefficients $u_{kn}(t)$ determined by discrete Fourier and Chebyshev transforms of the grid point values of u. The details of this procedure can be found in [9, 10]. In the temporal discretization, the pressure gradient term and the incompressibility constraint are best handled implicitly. So, too, are the vertical diffusion terms because of the fine mesh-spacing near the wall. The variable viscosity prevents the standard Poisson equation for the pressure from decoupling from the velocities in the diffusion term. A simple time discretization uses Crank–Nicholson on the implicit terms and second-order Adams–Bashforth on the remainder. After a discrete Fourier transform in x, the following set of ordinary differential equations and boundary conditions result

$$-\beta\hat{u}_{yy}^{n+1} + \hat{u}^{n+1} + i\hat{k}\hat{Q}^{n+1} = \hat{u}^n + \frac{\Delta t}{2}(3\hat{H}_1^n - \hat{H}_1^{n-1}) - i\hat{k}\hat{Q}^n + \beta\hat{u}_{yy}^n, \tag{2.7}$$

$$-\beta\hat{v}_{yy}^{n+1} + \hat{v}^{n-1} + \hat{Q}_y^{n+1} = \hat{v}^n + \frac{\Delta t}{2}(3\hat{H}_2^n - \hat{H}_2^{n-1}) - \hat{Q}_y^n + \beta\hat{v}_{yy}^n, \tag{2.8}$$

and

$$-i\hat{k}\hat{u}^{n+1} - \hat{v}_y^{n+1} = 0, \tag{2.9}$$

$$\begin{aligned} \hat{u}(-1) &= \hat{u}(+1) = 0, \\ \hat{v}(-1) &= \hat{v}(+1) = 0, \end{aligned} \tag{2.10}$$

where $\hat{k} = 2\pi k/L_x$, $\beta = \mu\Delta t/2$, $\hat{Q} = (\Delta t/2)\hat{P}$, $i = \sqrt{-1}$, and hats denote Fourier transformed variables in wavenumber space. The wavenumber is denoted by $\hat{k}$ and

the dependence of $\hat{u}$, $\hat{v}$, and $\hat{Q}$ upon $\hat{k}$ has been suppressed. The superscript n represents the time level. H_1 and H_2, which contain the terms treated explicitly, are given by

$$H_1 = -v(u_y - v_x) + (\mu u_x)_x + \mu_y u_y - P_x|_{\text{mean}} \tag{2.11}$$

$$H_2 = -u(v_x - u_y) + (\mu v_x)_x + \mu_y v_y. \tag{2.12}$$

The last term in Eq. (2.11) is the mean streamwise pressure gradient which drives the channel flow. All of these derivatives are evaluated by spectral collocation. A semi-implicit treament of the mean streamwise advection term is easily incorporated. For example, the left-hand side of Eq. (2.7) has the additive term

$$i\hat{k}\frac{\Delta t}{2} u_0 \hat{u}^{n+1};$$

in addition, $u_0 u_x$ appears in Eq. (2.11). Here, u_0 is the mean velocity.

For each wavenumber $\hat{k}$, the system of Eqs. (2.7)–(2.9) can be written, after a Chebyshev discretization in y, as

$$LU = F, \tag{2.13}$$

where $U = (\hat{u}^{n+1}, \hat{v}^{n+1}, \hat{Q}^{n+1})$ and F is the known right-hand side. The matrix L is a full $M \times M$ matrix where $M \cong 3N$. A direct solution of (2.13) by Gauss elimination methods would require $O(M^2)$ storage and $O(M^3)$ arithmetic operations. An iterative solution, on the other hand requires only $O(M)$ storage and $O(M \log M)$ operations per iteration. The description of an effective iterative scheme will be provided in the next section. The use of the variable $\hat{Q}$ in place of $\hat{P}$ puts L into a nearly self-adjoint form.

At this point some remarks pertinent to our selection of this scheme are in order. Our goal was to develop a single, fully spectral algorithm which is applicable to a broad class of problems. Many interesting phenomena involve a strong variation of the viscosity, the mean advection, and/or the geometric terms in the direction normal to the wall (or walls) and possibly also in time. (A number of 3-dimensional calculations employing the present algorithm on such problems are in progress and will be reported elsewhere.) In many of these problems semi-implicit treatment of the normal diffusion and/or the mean streamwise advection are desirable. The observations of Marcus [6] about the pitfalls of the time-splitting in some problems is a strong argument in favor of an unsplit method for a general purpose algorithm. A Chebyshev τ method in the normal direction is ruled out in favor of Chebyshev collocation in all but the simplest cases. The variable viscosity and mean advection prevent the velocity and pressure equations from decoupling as in the influence matrix methods [3, 6]. The matrix diagonalization technique for solving Eq. (2.13) is not practical because the matrix L may depend upon time. These considerations have led us to develop an iterative technique for solving the collocation equations.

3. Spectral Solution with Finite Difference Preconditioning

The key to the efficiency of an iterative method for the solution of Eq. (2.13) is the use of an effective preconditioning matrix so that the number of iterations is small. The reason is that the condition number of the matrix L is large. Consequently, standard iterative techniques would be slow. But let H be some preconditioning matrix for L, i.e., the iterative scheme is, in effect, applied to the equation

$$H^{-1}LU = H^{-1}F.$$

The desirable properties of the preconditioning matrix are that the condition number of $H^{-1}L$ be small and that equations such as

$$HU = G$$

can be solved cheaply for U (relative to the evaluation of LU). The first property implies that only a small number of iterations are required and the second property implies that a single preconditioned iteration costs roughly the same as a single unpreconditioned iteration. We base our choice of H on Orszag's suggestion [11] that a finite difference approximation to the differential equation be used. The interesting physical problems have high Reynolds numbers, i.e., low viscosity. Thus, the first derivative terms in Eqs. (2.7)–(2.9) predominate. Therefore, their effective preconditioning is crucial.

To illustrate the difficulty with first derivative terms and to assess various remedies we consider the model scalar problem

$$u_x = f \tag{3.1}$$

on $[0, 2\pi]$ with periodic boundary conditions. The appropriate spectral method uses Fourier collocation. The eigenfunctions of the discrete spectral operator L and of the finite difference operator H are the exponentials

$$e^{ikx_j}$$

where k is the wavenumber and x_j is a Fourier collocation point as given by Eq. (2.4). Four possibilities for the finite difference operator are considered here: central differences, central differences with a high mode cutoff, one-sided differences, and the use of a staggered mesh. The effect of the staggered grid is modelled by evaluating the spectral residual at the points $x_{j+1/2} = 2\pi(j+\frac{1}{2})/N$ rather than at the points $x_j = 2\pi j/N$. The eigenvalues of these preconditioned matrices, $H^{-1}L$, for the model scalar problem are given in Table I for all four possibilities. The term $k\Delta x$ is the product of the wavenumber k and the grid spacing Δx. It falls in the range $|k\Delta x| < \pi$. The eigenvalues for the centered differences $k\Delta x/\sin k\Delta x$, are unbounded as $|k\Delta x| \to \pi$. Thus, pure central difference preconditioning yields a large condition number for $H^{-1}L$. Orszag [11] noted that truncating the high modes limit the

eigenvalues. Table I indicates that this does produce a bounded spectrum; the price is that some high wavenumber information is lost. Another cure is to use one-sided (forward or backward) differences for the first derivative terms. For the model problem, it results in bounded but complex eigenvalues with real parts tending to zero. Many iterative schemes perform badly on such problems. For the staggered mesh the eigenvalues of the preconditioned matrix for the model problem remain bounded and real, with no loss of high wavenumber information.

These model problem results led us to consider a staggered mesh for the Navier–Stokes equations. The staggered mesh which is appropriate for the Fourier–Chebyshev discretization is staggered only in the y direction. The velocities are defined at the cell faces y_m, as given by Eq. (2.5), and the pressure is defined at the cell centers

$$y_{m-1/2} = \cos(\pi(m - \tfrac{1}{2})/N), \qquad m = 1, \ldots, N. \tag{3.2}$$

The momentum equations are enforced at the faces, whereas the continuity equations are enforced at the centers. The velocity boundary conditions are enforced at the two walls. Note that there is no need for an artificial pressure boundary condition at the walls.

The staggered mesh assigns one less vertical degree of freedom to the pressure than to the velocities. This is common practice in finite element techniques for the Navier–Stokes equations (see, e.g., [12]). Huberson and Morchoisne [13] have recently proposed a filtering procedure for spectral solutions of the incompressible Navier–Stokes equations on a non-staggered mesh. It has the effect of removing one vertical degree of freedom from the pressure.

Let us now examine some of the details involved in employing a staggered mesh for Eqs. (2.7)–(2.9). Focus first on the spectral evalutions of the various terms. The

TABLE I

Preconditioned Eigenvalues for One-Dimensional First Derivative Model Problem

Preconditioning	Eigenvalues
Central differences	$\dfrac{k\Delta x}{\sin(k\Delta x)}$
High mode cutoff	$\dfrac{k\Delta x}{\sin(k\Delta x)}$ $\quad \lvert k\Delta x\rvert \leqslant (2\pi/3)$ 0 $\quad (2\pi/3) < \lvert k\Delta x\rvert \leqslant \pi$
One-sided differences	$e^{-i(k\Delta x/2)} \dfrac{k\Delta x/2}{\sin((k\Delta x)/2)}$
Staggered grid	$\dfrac{(k\Delta x)/2}{\sin((k\Delta x)/2)}$

explicit terms, denoted by H_1 and H_2, are evaluated in a straightforward manner since they are required at the faces and involve only the velocities. The same holds for the remaining velocity terms in the momentum equations. The only complication here is the two terms involving the pressure. From the values of Q at the centers, trigonometric interpolation can be used to obtain Q at the faces. First, use the center values to obtain the Chebyshev coefficients

$$\hat{P}_n = \frac{2}{N} \sum_{m=1}^{N} \hat{P}(y_{m-1/2}) \cos \frac{\pi n(m-\frac{1}{2})}{N} m \tag{3.3}$$

for $n = 0, 1, \ldots, N-1$, where the dependence upon $\hat{k}$ and t has been suppressed. Then set $\hat{Q}_N = 0$ and compute the values of $\hat{Q}$ at the faces

$$\hat{Q}(y_m) = \sum_{n=0}^{N} \hat{Q}_n \cos \frac{\pi mn}{N}, \qquad m = 0, 1, \ldots, N. \tag{3.4}$$

Both of these sums may be computed by fast cosine transforms. This takes care of the pressure term in Eq. (2.7). The $\hat{Q}_y$ term in Eq. (2.8) may be evaluated from the values of $\hat{Q}$ at the faces in a standard fashion. For the continuity equation one first evaluates

$$\hat{r} = i\hat{k}\hat{u} + \hat{v}_y$$

at the cell faces in the standard manner and then interpolates this result to the cell centers, via

$$\hat{r}_n = \frac{2}{N\bar{c}_n} \sum_{m=0}^{N} \bar{c}_m^{-1} \hat{r}(y_m) \cos \frac{\pi nm}{N} \tag{3.5}$$

for $n = 0, 1, \ldots, N$ where

$$\begin{aligned} \bar{c}_n &= 2, \qquad n = 0 \text{ or } N \\ &= 1, \qquad 1 \leqslant n \leqslant N-1, \end{aligned} \tag{3.6}$$

and

$$\hat{r}(y_{m-1/2}) = \sum_{n=0}^{N} \hat{r}_n \cos \frac{\pi(m-\frac{1}{2})n}{N}, \qquad m = 1, \ldots, N. \tag{3.7}$$

The finite difference operator H pertains only to the left-hand side of Eqs. (2.7)–(2.9). The second derivative of the velocities is evaluated by 3-point centered differences of the values at the faces, using the formula appropriate for the non-uniform grid, e.g.,

$$\hat{u}_{yy}\Big|_m = \frac{2}{y_{m+1} - y_{m-1}} \left[\frac{\hat{u}_{m+1} - \hat{u}_m}{y_{m+1} - y_m} - \frac{\hat{u}_m - \hat{u}_{m-1}}{y_m - y_{m-1}} \right].$$

The pressure term in the u momentum equation is approximated by a linear average of the adjacent cell-centered pressure values. The vertical pressure gradient term in the v momentum equation is approximated by 2-point differences of the adjacent cell-centered pressure values. The streamwise velocity in the continuity equation is taken as the linear average of the velocity values at adjacent cell faces and the vertical derivative of $\hat{v}$ uses 2-point differences of the adjacent cell faces values. Order the unknowns as

$$U = (\hat{u}_1, \hat{v}_1, \hat{Q}_{1/2}, \hat{u}_2, \hat{v}_2, \hat{Q}_{3/2}, \ldots, \hat{u}_N, \hat{v}_N, \hat{Q}_{N-1/2})$$

and order the equations as

continuity at $y_{1/2}$
v momentum at y_1
u momentum at y_1
$\vdots$
continuity at $y_{N-3/2}$
v momentum at y_{N-1}
u momentum at y_{N-1}

u BC at y_N
v BC at y_N
continuity at $y_{N-1/2}$.

This requires the velocity boundary conditions at y_0 to be absorbed into the matrix. This ordering produces a block tridiagonal structure for H that can evidently be solved without pivoting within the diagonal block. (We have no proof for this claim, but we have made numerous checks. In all cases the solution without pivoting produced results that agreed with solutions with pivoting to at least eight digits.)

For $\hat{k} = 0$ the structure is even simpler. The velocity $\hat{v}$ is constant in y, the velocity $\hat{u}$ satisfies a tridiagonal equation, and the pressure $\hat{Q}$ satisfies a bidiagonal equation. The latter is solved by setting $\hat{Q}(y_{1/2}) = 0$ and then solving for each successive value of pressure. This particular choice of $\hat{Q}(y_{1/2})$ is arbitrary and corresponds to specifying the mean level of pressure.

We have computed eigenvalues of $H^{-1}L$ not only for the staggered grid method but also for the same three alternatives that were discussed for the model problem. In these cases the pressure is defined at the cell faces and the continuity equation is enforced at the cell faces. This version requires numerical boundary conditions for the pressure at the walls. The continuity equation and the vertical momentum equation yield

$$\hat{P}_y = -i\hat{k}(\mu\hat{u})_y.$$

The finite difference approximation uses one-sided differences and the matrix H is still block tridiagonal.

The eigenvalues of the preconditioned matrix $H^{-1}L$ for the Navier–Stokes equations are displayed in Figs. 1 and 2 for two wavenumbers and for four different discretizations of the first derivative terms.

The results for $\hat{k}=1$ are particularly interesting. When central differences for the first derivative terms are used, there are several complex eigenvalues with large real parts. The remaining eigenvalues are real with $1.0 \leqslant \lambda \leqslant 4.5$. As N increases, both the real and imaginary parts of the eigenvalues grow. (The largest eigenvalues for $N=24$ and 32 are $12.3 \pm i\ 4.5$ and $16.5 \pm i\ 6.4$, respectively.) When the upper one-

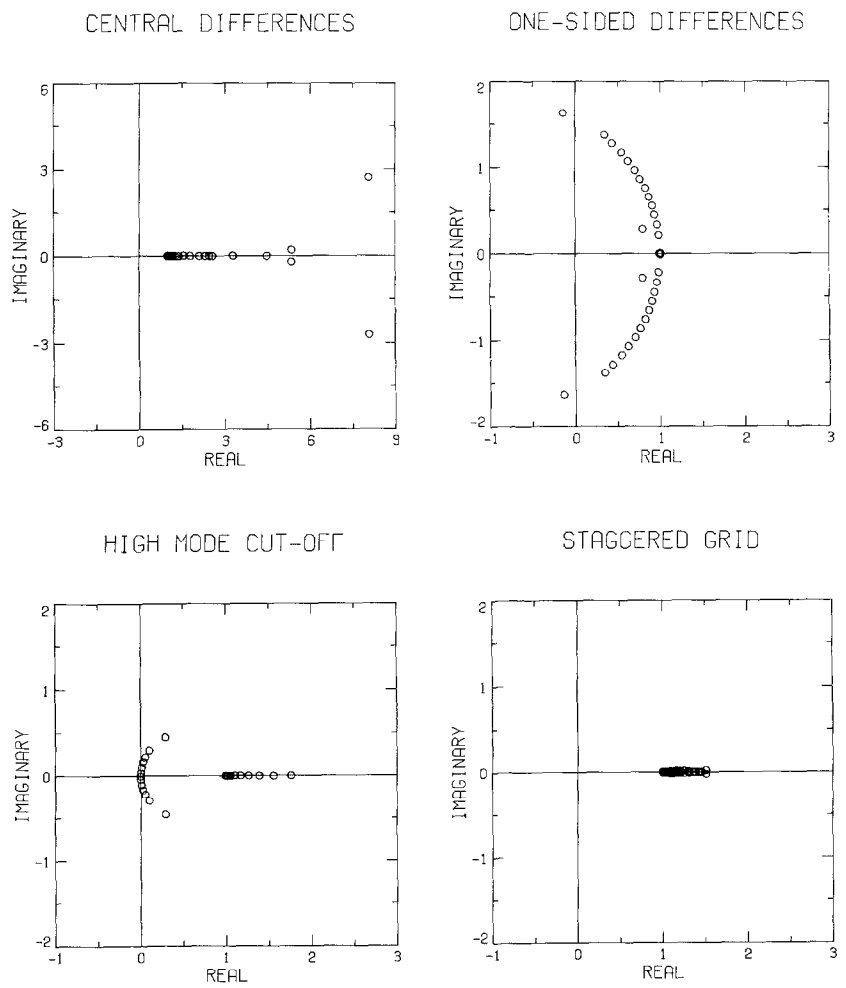

FIG. 1. A plot of $\hat{k}=1$ channel flow eigenvalues of the preconditioned matrix $H^{-1}L$ for four first derivative treatments. In this case $\mu^{-1}=7500$, CFL $=0.1$, $N=16$, and $K=32$.

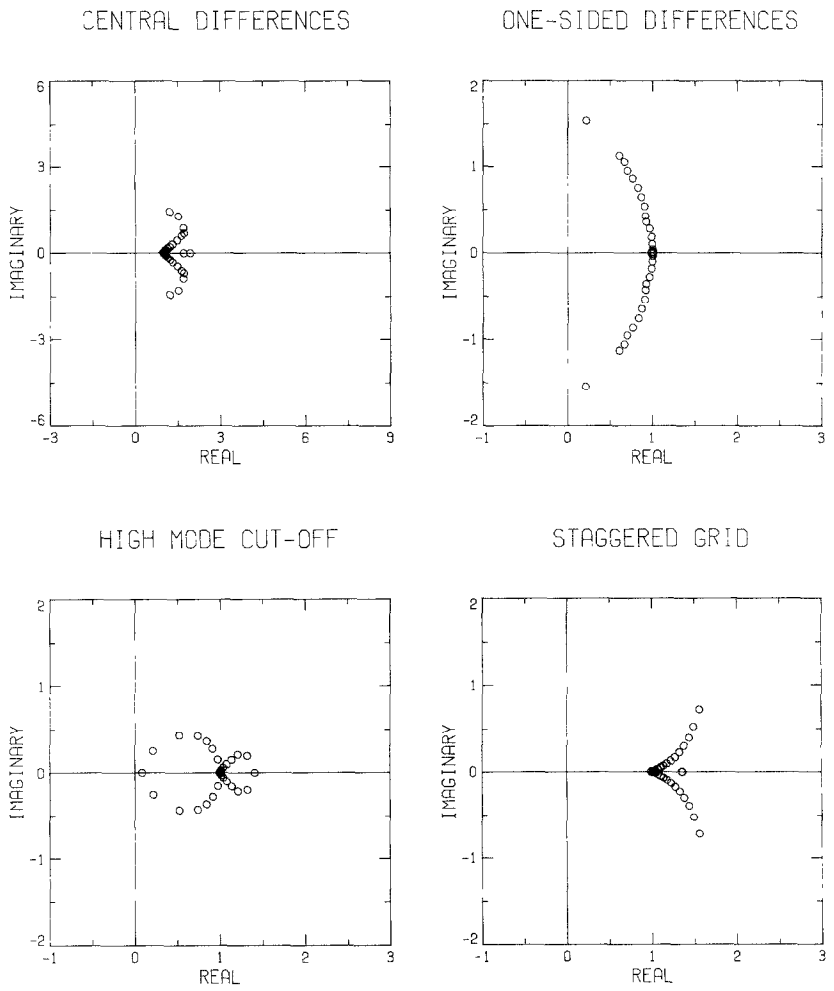

FIG. 2. A plot of $\hat{k} = 10$ channel flow eigenvalues of the preconditioned matrix $H^{-1}L$ for four first derivative treatments In this case $\mu^{-1} = 7500$, CFL $= 0.1$, $N = 16$, $K = 32$.

third of the Chebyshev modes are cut off in the first derivative representation the spectrum is apparently bounded from above. However, there are now a number of complex eigenvalues with small real parts. One-sided first differences yield mainly complex eigenvalues including some with very small positive real parts. When the mesh is staggered, all the eigenvalues for $\hat{k} = 1$ lie close to the real axis between 1 and $\pi/2 \cong 1.57$.

The eigenvalue spectra are only slightly different at higher wavenumbers, as illustrated in Fig. 2 for $\hat{k} = 10$. Although there are some complex eigenvalues for the staggered mesh, they are reasonably well confined. Similar eigenvalue calculations have been performed for the staggered grid algorithm for $N = 24$ and $N = 32$. The

real parts are still confined between 1 and $\pi/2$ and the magnitudes of the imaginary parts decrease as N increases.

Note that the model problem estimates the eigenvalue trends surprisingly well considering that it is just a scalar equation, has only first derivative terms, and uses Fourier series rather than Chebyshev polynomials.

The preceding results indicate that the staggered grid leads to the most effective treatment of the first derivative terms. The condition number of the preconditioned system is reasonably small and full resolution is retained. However, the iterative scheme used for solving Eqs. (2.7)–(2.9) must be capable of dealing with the complex eigenvalues. Two types of iterative schemes are feasible. Chebyshev iteration [14] will converge because the real parts of the eigenvalues are greater than 1. However, this method contains parameters that depend upon the location of the eigenvalues in the complex plane. Alternatively, a parameter-free variational method [15] such as the minimum residual (MR) method will work provided that the Hermitian part of LH^{-1} is positive definite. Provided that the pressure term and the continuity equation are divided by $\hat{k}$, for $\hat{k} \neq 0$, this condition is satisfied for all the cases discussed in this paper.

The preconditioned version of MR for Eq. (2.13) involves making an initial guess U^0, computing the initial residual

$$R^0 = F - LU^0, \tag{3.8}$$

solving

$$HZ^0 = R^0, \tag{3.9}$$

and then iterating according to

$$\alpha_l = \frac{(LZ^l, R^l)}{(LZ^l, LZ^l)} \tag{3.10}$$

$$U^{l+1} = U^l + \alpha_l Z^l \tag{3.11}$$

$$R^{l+1} = R^l - \alpha_l LZ^l \tag{3.12}$$

$$Hz^{l+1} = R^{l+1} \tag{3.13}$$

until convergence. The parameter α_l in Eq. (3.10) is chosen so that the residual in Eq. (3.12) is as small as possible consistent with the prescription (3.11). Representative convergence histories for the MR method are shown in Fig. 3 where the L_1 norm of the residual for $\hat{k} = 1$ is plotted against number of iterations for $N = 16$, 32, and 64. In this case, $K = 4$. At a Reynolds number of 7500, each iteration is found to reduce the residual by almost an order of magnitude and thee is a trend of faster convergence with increasing N which may be partly attributed to the higher resolution. In a fully nonlinear calculation, it is important that the convergence for the higher modes should also be fast. A comparison of the convergence histories for

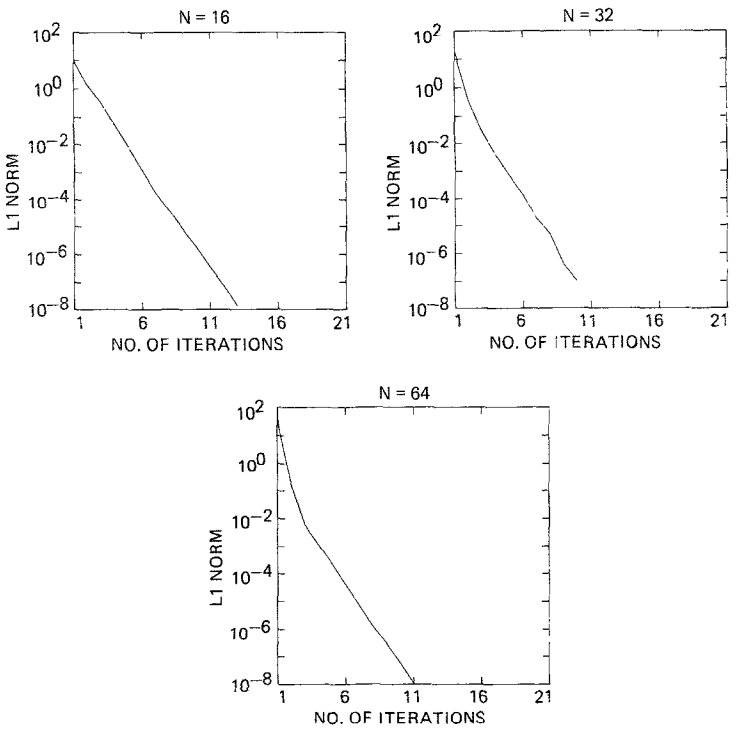

FIG. 3. Convergence history of the minimum residual method for the channel flow problem ($\mu^{-1} = 7500$) for $\hat{k} = 1$ using $K = 4$.

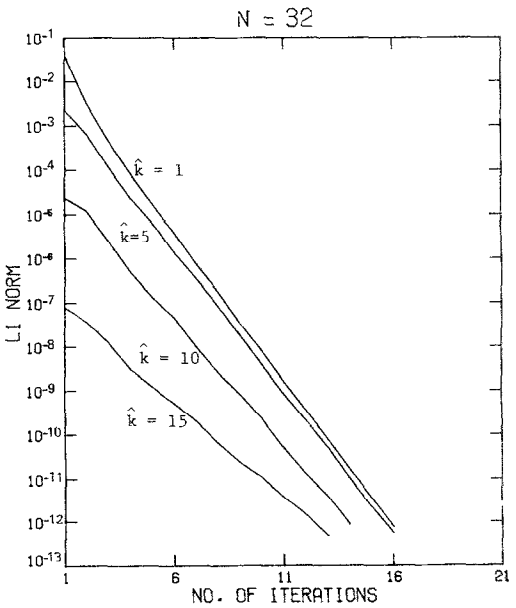

FIG. 4. Convergence history of the minimum residual method for the channel flow problem (μ^{-1} 7500) for $\hat{k} = 1$, 5, 10, and 15 using $K = 32$.

$\hat{k} = 1$, 5, 10, and 15 is made in Fig. 4. This calculation was done with $N = K = 32$. While the convergence tends to slow down at higher modes, the residue still decreases by a factor of 3–4 after each iteration.

The physical results to be presented in Fig. 6 and Table III become intensive when the L_1 norm is smaller than 10^{-6}.

4. Evolution of Small Disturbances in Channel Flow

In order to test the algorithm proposed for Navier–Stokes equations, we study the problem of the evolution of small disturbances in channel flow. This problem has been studied extensively using the Orr–Sommerfeld equation. When the amplitude of the disturbances imposed upon the mean (time independent) channel flow $u(y) = (1 - y^2)$ is small, then the numerical solution of the Navier–Stokes equation should be the same as that implied by the Orr–Sommerfeld solution. This linear solution has the form

$$u(x, y, t) = (1 - y^2) + \varepsilon \operatorname{Re}\{\psi_y(y)\, e^{i(\alpha x - \omega t)}\}, \tag{4.1}$$

$$v(x, y, t) = -\varepsilon \operatorname{Re}\{i\alpha\psi(y)\, e^{i(\alpha x - \omega t)}\}, \tag{4.2}$$

where ψ is the eigenfunction normalized to a maximum value of 1, ω is the complex frequency (with the largest imaginary part), α is the prescribed wavenumber, and ε is the perturbation amplitude.

The perturbation flow energy $E(t)$ is

$$E(t) = \int_0^{L_x} dx \int_{-1}^{1} \{[u(x, y, t) - (1 - y^2)]^2 + v^2(x, y, t)\}\, dy, \tag{4.3}$$

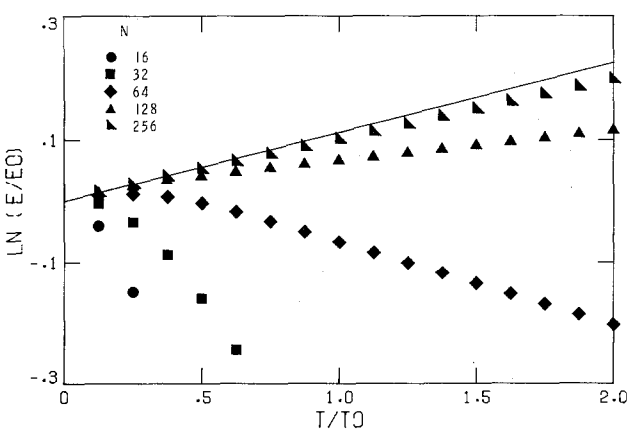

FIG. 5. Computed perturbation energy ratio for channel flow problem ($\mu^{-1} = 7500$). A Fourier spectral method in x and a second-order finite difference method in y are used. Results are shown for a 4-point grid in x and for various grids in y. The solid line is the correct result.

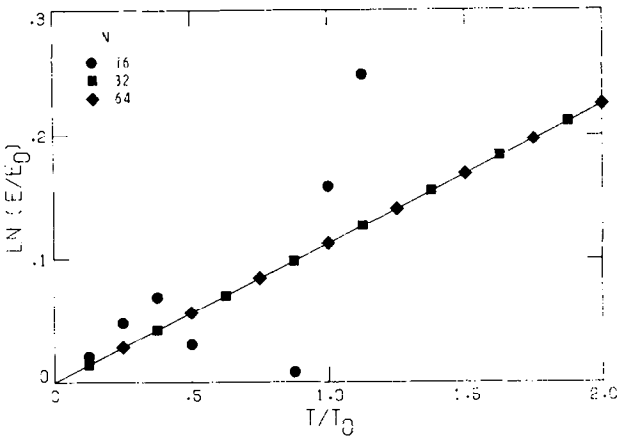

FIG. 6. Computed perturbation energy ratio for channel flow problem ($\mu^{-1} = 7500$). A Fourier spectral method in x and a Chebyshev spectral method in y are used. Results are shown for a 4-point grid in x and for various grids in y. The solid line is the correct result.

where $L_x = 2\pi/\alpha$. Choose initial conditions from Eqs. (4.1) and (4.2) with $t = 0$ and let $E_0 = E(0)$. For small amplitudes $E(t)/E_0 = e^{2\omega_i t}$.

The particular problem chosen for study had $\mu = (7500)^{-1}$ and $\alpha = 1$. The only unstable mode has $\omega = 0.24989154 + i\ 0.00223498$. The amplitude parameter was $\varepsilon = 0.0001$. Two different discretizations in y were used: (1) Chebyshev collocation

TABLE II

Channel Fourier-Finite Difference Convergence

1 Period

N	$E_f/E_0\|_{\text{calc}}$	$E_f/E_0\|_{\text{error}}$
16	0.31369085	−0.80526006
32	0.59348926	−0.52546165
64	0.93539768	−0.18355323
128	1.06837752	−0.05057339
256	1.10598936	−0.01296155

2 Periods

N	$E_f/E_0\|_{\text{calc}}$	$E_f/E_0\|_{\text{error}}$
16	0.45883275	−0.79321839
32	0.26725477	−0.98479637
64	0.81641093	−0.43564021
128	1.12221673	−0.12983441
256	1.21820807	−0.03384307

and (2) finite differences. Both methods used a Fourier collocation method in x. The Fourier-finite difference method used a staggered mesh, with the cell centers given by Eq. (3.2) and the cell faces located midway between the neighboring cell centers. This method is just that of Moin and Kim [7], applied to a direct simulation. Only four collocation points were used in the x direction. For this basically linear test problem, the x direction has essentially perfect resolution. The time step was small enough so that the vertical discretization errors were predominant in all but the most highly resolved cases.

The basic comparison of the vertical discretizations is provided in Figs. 5 and 6, where the natural logarithm of the perturbation energy ratio is plotted. The solid line in the figures represents the linear stability result. The finite difference solution is plotted in Fig. 5 for several vertical grids. Even the $N = 256$ results are appreciably in error.

The Fourier–Chebyshev results are presented in Fig. 6. The results for the $N = 32$ grid are already in excellent agreement with the linear theory results. The numerical results for $N = 16$ are wildly inaccurate. This is in contrast with the finite difference calculations where $\ln E/E_0$ at least varies linearly with the time for various grids. This behaviour is typical of spectral methods in general: if the resolution is inadequate, say worse than 20%, then the spectral results are inferior to finite difference results; however, once the 10% accuracy level is achieved, spectral results become dramatically superior.

In the above calculations, all runs were terminated at $t/t_0 = 2$, where t_0 is the time required for the wave to propagate through the streamwise computational domain. In this case, $t_0 = 25.1438$. The calculated energy ratio and its error at one and two periods are represented in Tables II and III for the finite difference and the Chebyshev methods, respectively. The convergence of the finite difference method is

TABLE III

Channel Fourier–Chebyshev Convergence

1 Period

N	$E_f/E_0\|_{\text{calc}}$	$E_f/E_0\|_{\text{error}}$
16	1.17188803	0.05293712
32	1.11912239	0.00017148
64	1.11896735	0.00001644

2 Periods

N	$E_f/E_0\|_{\text{calc}}$	$E_f/E_0\|_{\text{error}}$
16	2.07329163	0.82124050
32	1.25291992	0.00086879
64	1.25214542	0.00009429

quadratic. The convergence of the Chebyshev method is dramatic: the $N=32$ spectral results are far better than $N=256$ finite difference results (and took less CPU time). The error for the $N=64$ Chebyshev case is dominated by time discretization and nonlinear effects.

The spectral results were all obtained with a time step corresponding to a mean streamwise CFL number of 0.025 and with an explicit treatment of advection. Such a small time step is necessary for accuracy purposes. Stability problems over two periods only arise for CFL numbers above 0.30. The advantage of the capability of the algorithm to treat the mean advection implicitly arises in calculations with higher spatial resolution. An example is provided by calculations for this same test problem using 16 Fourier modes rather than 4. The semi-implicit advection version of the algorithm is stable for CFL numbers as large as 1. However, the accuracy suffers for such large time steps.

5. Discretization for External Boundary Layers ($0 \leqslant y \leqslant \eta_\infty$)

This numerical method may also be applied to a model of the external boundary layer. In order to use periodic boundary conditions in the streamwise direction, one must make the parallel flow assumption, i.e., fix on some reference location in a spatially growing boundary layer and use the corresponding mean velocity profile at all x. One must then set the mean vertical velocity to zero and make a minor adjustment to the mean streamwise pressure gradient to achieve parallel flow.

A stretching transformation can be applied in the (unbounded) vertical direction. Let

$$y = a\frac{1+\xi}{b-\xi}, \tag{5.1}$$

where y is the physical vertical coordinate, ξ is the computational coordinate and a and b are constants. Let η_∞ be the upper boundary in the physical plane and set

$$b = 1 + \frac{2a}{\eta_\infty}. \tag{5.2}$$

Then for any choice of the scaling parameter a, the computational coordinate ξ, falls within the standard Chebyshev interval $[-1, 1]$. Derivatives in the vertical direction are evaluated by multiplying the Chebyshev collocation derivative in ξ by the Jacobian of the transformation, i.e.,

$$\hat{u}_y = \frac{d\xi}{dy}\hat{u}_\xi. \tag{5.3}$$

The necessary modifications to Eqs. (2.7)–(2.12) are straightforward.

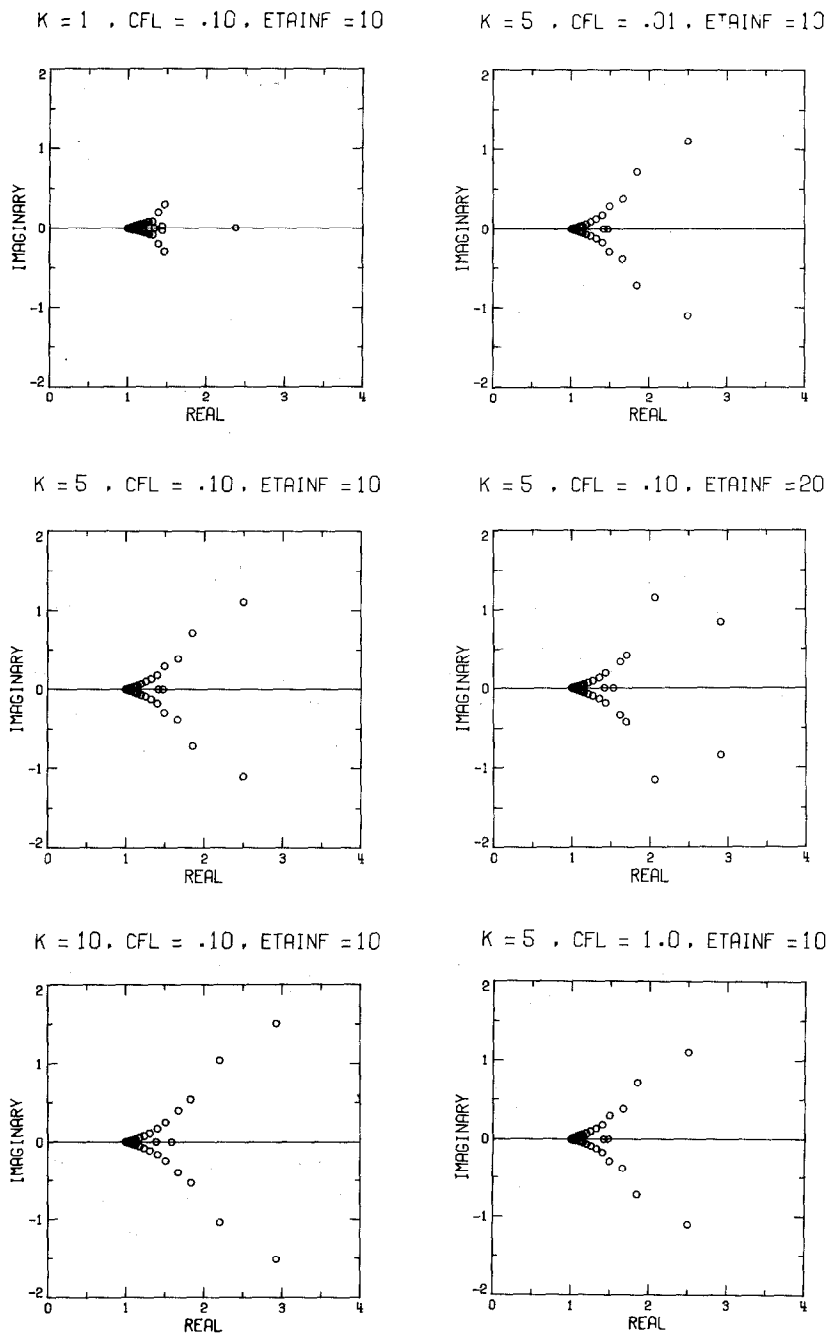

FIG. 7. A plot of the eigenvalues of the preconditioned matrix $H^{-1}L$ for an external boundary layer using the staggered grid. In this case, $\mu^{-1} = 1500$, $N = 16$, and $K = 32$. Zeroth-order boundary conditions

A number of choices are available for the numerical boudary condition at η_∞. The simplest is to require that the solution at $y=\eta_\infty$ correspond to the flow at infinity. This is accomplished by setting $\hat{u}$ at $y=\eta_\infty$ for $\hat{k}=0$ equal to the free stream velocity and setting all other velocity components to zero. Another approximation was used by Fasel [16] in his finite difference calculations of the boundary layer:

$$\begin{aligned} \hat{u}_y &= -|\hat{k}|\,\hat{u} \\ \hat{v}_y &= -|\hat{k}|\,\hat{v}. \end{aligned} \tag{5.4}$$

These two alternatives will be referred to below as the zeroth-order and first-order boundary conditions, respectively.

The finite difference preconditioning matrix is straightforward. Both types of upper boundary conditions lead to a block tridiagonal structure for H (which does not appear to require pivoting). The eigenvalues for the preconditioned matrix are

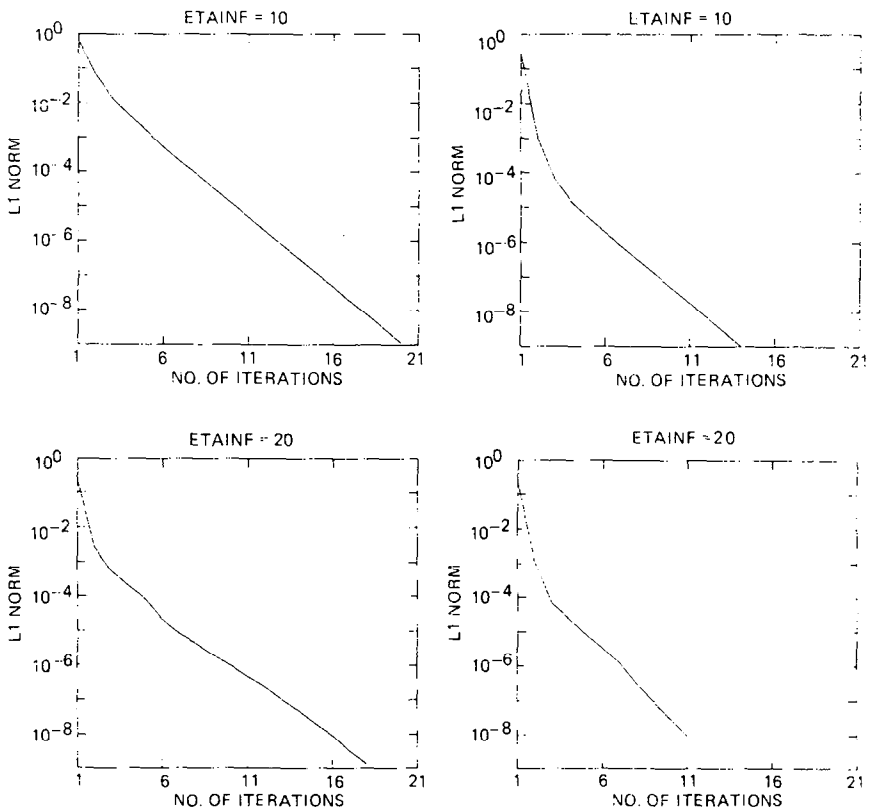

FIG. 8. Convergence history of the minimum residual method for the boundary layer problem. Zeroth-order boundary conditions are used in the parts of the figure on the left-hand side and first-order conditions in parts on the right-hand side.

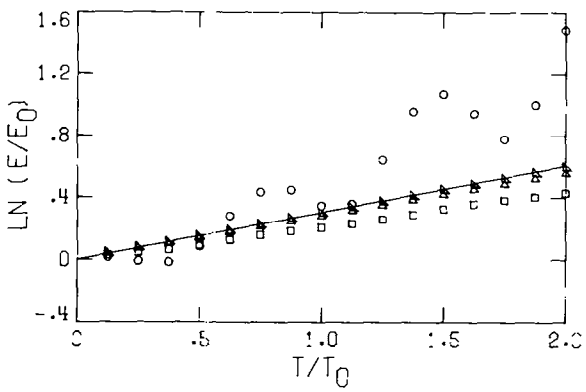

FIG. 9. Computed perturbation energy ratio for the boundary layer problem with constant viscosity ($\mu^{-1} = 1500$). A Fourier spectral method in x and a second-order finite difference method in y are used. Results are shown for a 4-point grid in x and various grids in y ($N = 32$ (○), 64 (□), 128 (△), 256 (▷)). The solid line is the correct result.

illustrated in Fig. 7. The grid has $K = 32$, $N = 16$, and the Reynolds number (μ^{-1}) is 7500. The stretching parameter a (see Eq. (5.1)) is chosen such that about 55% of the nodes lie in the region $0 \leqslant y \leqslant 2$ and the rest lie in $2 \leqslant y \leqslant \eta_\infty$. Three different CFL numbers (0.01, 0.1, 1.0) are checked and the effect is found to be negligible. The eigenvalues do tend to become widely apart with increasing η_∞. For fast convergence, therefore, one would like to impose the freestream boundary conditions at as small η_∞ as possible. Representative convergence histories of the MR method for the boundary layer case are shown in Fig. 8. Boundary conditions are imposed at $\eta_\infty = 10$ and 20. Both the zeroth- and first-order boundary conditions are used and the convergence is found to be significantly faster in the latter case. The physical results to be presented become insensitive when the L_1 norm is smaller than 10^{-6}.

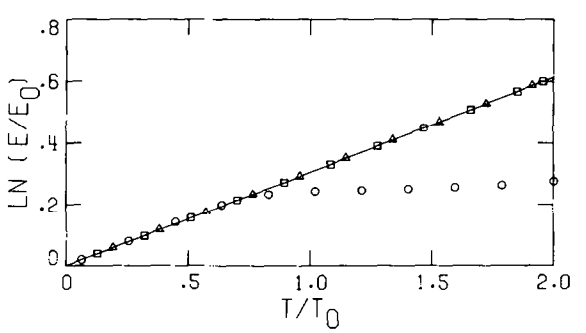

FIG. 10. Computed perturbation energy ratio for the boundary layer problem. A Fourier spectral method in x and a Chebyshev spectral method in y are used. Results are shown for a 4-point grid in x and various grids in y ($N = 16$ (○), 32 (□), 64 (△)). The solid line is the correct result. In this case, zeroth-order boundary conditions are imposed at $\eta_\infty = 20$.

TABLE IV

Boundary Layer Fourier-Finite Difference Convergence

1 Period

N	$E_f/E_0\|_{\text{calc}}$	$E_f/E_0\|_{\text{error}}$
32	1.4144405	0.05899918
64	1.2294246	−0.12601673
128	1.3213179	−0.03412346
256	1.3469941	−0.00844721

2 Periods

N	$E_f/E_0\|_{\text{calc}}$	$E_f/E_0\|_{\text{error}}$
32	4.4395339	2.6023126
64	1.5376562	−0.29956505
128	1.7459684	−0.09125289
256	1.8144658	0.02275544

We now describe results of computations of the evolution of small disturbances in flat plate flow with no-slip boundary conditions at the solid wall. The initial conditions are the Orr–Sommerfeld solution imposed upon the Blasius profile. The vertical grid y is normalized with respect to the boundary layer displacement thickness.

The particular problem chosen for study had $\mu = (1500)^{-1}$, $\alpha = 0.3$, and $\omega = 0.10288548 + i\ 0.00249003$. The zeroth-order boundary conditions were imposed at $\eta_\infty = 20$, i.e., 20 displacement thicknesses. The amplitude parameter ε is taken to be

TABLE V

Boundary Layer Fourier–Chebyshev Convergence

1 Period

N	$E_f/E_0\|_{\text{calc}}$	$E_f/E_0\|_{\text{error}}$
16	1.2760938	−0.07934649
32	1.3554140	0.00002630
64	1.3554399	−0.00000040

2 Periods

N	$E_f/E_0\|_{\text{calc}}$	$E_f/E_0\|_{\text{error}}$
16	1.3200385	−0.51718473
32	1.8376986	0.00048000
64	1.8372536	0.00003501

TABLE VI

Effect of η_∞ and Top Boundary Condition

	$E_f/E_0\|_{\text{error}}$			
	$\eta_\infty = 10$		$\eta_\infty = 20$	
N	0th order	1st order	0th order	1st order
16	−0.21312422	0.16289710	−0.51718473	−0.52723330
32	−0.09173191	0.00023775	0.00048000	0.00021268

TABLE VII

Orr–Sommerfeld Solution for Water Boundary Layer with Wall Heat Transfer ($\alpha = 0.15$, $(\mu_\infty)^{-1} = 10{,}000$)

θ_w/θ_∞	ω	t_0
1.1	$0.02872049 + i\,0.00020520$	218.7701
1.0	$0.03386607 + i\,0.00343206$	185.5303
0.9	$0.03445962 + i\,0.01259238$	182.3347

TABLE VIII

Navier–Stokes Solution for Water Boundary Layer with Wall Heat Transfer ($\eta_\infty = 20$, $N = 32$, 1st order B.C.)

1 period

θ_w/θ_∞	$E_f/E_0\|_{\text{calc.}}$	$E_f/E_0\|_{\text{error}}$
1.1	1.0946078	0.00067076
1.0	3.5720516	−0.00127094
0.9	99.374109	0.67521093

2 Periods

θ_w/θ_∞	$E_f/E_0\|_{\text{calc.}}$	$E_f/E_0\|_{\text{error}}$
1.1	1.1972253	0.00052696
1.0	12.757289	−0.01134543
0.9	9871.3827	129.91024

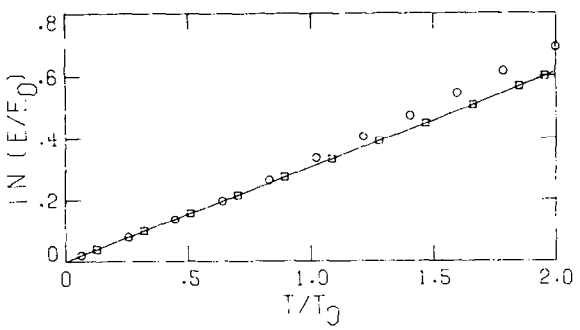

FIG. 11. Computed perturbation energy ratio for the boundary layer problem. A Fourier spectral method in x and a Chebyshev spectral method in y are used. Results are shown for a 4-point grid in x and two different grids in y ($N = 16$ (○), 32 (□)). The solid line is the correct result. In this case, first-order boundary conditions are imposed at $\eta_\infty = 10$.

0.0001. Four Fourier spectral modes were used in the streamwise direction. All runs were terminated at $t/t_0 = 2$, where t_0 is the time required for the wave to propagate through the streamwise grid. In this case $t_0 = 61.0689$.

Results analogous to those provided earlier for channel flow are given in Figs. 9 and 10 and Tables IV and V. The $N = 32$ finite difference results are oscillatory in time as shown in Fig. 9. This caused the results presented in Table IV for one period to wrongly suggest that the error for $N = 64$ is higher than that for $N = 32$. The $N = 32$ Chebyshev results are far more accurate than the $N = 256$ finite difference results and required less CPU time. Some additional Fourier–Chebysev calculations were performed to assess the upper boundary conditions. The results are reported in Table VI in terms of the energy error after two periods. For $\eta_\infty = 10$, first-order boundary conditions provide a significant improvement in

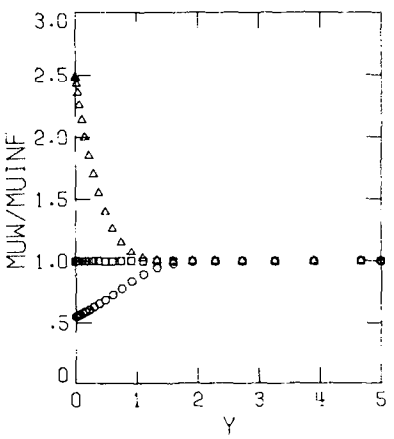

FIG. 12. Variation of viscosity for a water boundary layer with and without wall heat transfer ($\theta_\infty = 293°K$) ($\theta_w/\theta_\infty = 1.1$ (○), 1.0 (□), 0.9 (△)).

accuracy over the zeroth-order ones. At $\eta_\infty = 20$, however, the improvement is marginal. The results for first-order boundary conditions at $\eta_\infty = 10$ are plotted in Fig. 11. Significant improvement for $N = 16$ can be noted in comparison with Fig. 10 where zeroth-order boundary conditions were imposed at $\eta_\infty = 20$.

In order to test the variable viscosity capability of the numerical algorithm, we applied it to water boundary layers with wall heat transfer. The viscosity of water is a strong function of temperature, decreasing with increasing temperature. Thus, heating of water boundary layers has a stability effect. We used the empirical temperature–viscosity formula given in [17].

An Orr–Sommerfeld equation for incompressible flow to include the effect of viscosity can be derived as in [18] by neglecting temperature perturbations. This equation has been solved to provide initial conditions for the Navier–Stokes code which also neglects the temperature perturbation. The free stream temperature θ_∞ is assumed to be 293°K and three wall-to-freestream temperature ratios were examined: $\theta_w/\theta_\infty = 1.1$, 1.0, 0.9. The resulting viscosity distributions calculated are plotted in Fig. 12. The freestream Reynolds number $(\mu_\infty)^{-1} = 10000$ and $\alpha = 0.15$. The Orr–Sommerfeld eigenvalues and time periods (t_0) for the three cases are given in Table VII. The Navier–Stokes solutions for the three temperature ratios are presented in Fig. 13. The solution has been obtained with first-order boundary conditions imposed at $\eta_\infty = 20$ and using $N = 32$. In each case 500 time steps were used to reach $t/t_0 = 2$. The solid line in each case represents the theoretical results. While the growth rates are vastly different for the three cases, the calculated results are in

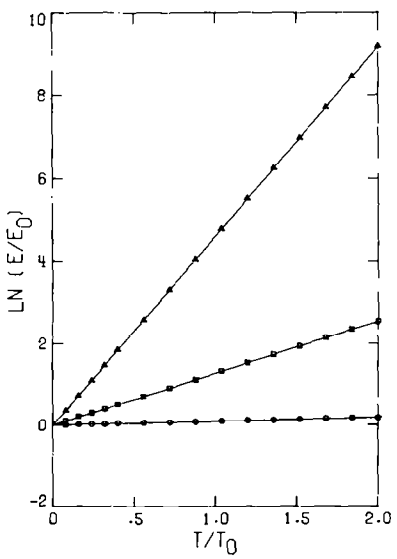

FIG. 13. Computed perturbation energy ratio for a water boundary layer ($\mu_\infty^{-1} = 10{,}000$) using a Fourier–Chebyshev spectral method. The results shown are for a 4-point grid in x and a 33-point grid in y. $\theta_w/\theta_\infty = 1.1$ (○), 1.0 (□), 0.9 (△) pertain to wall heating, no heating, and wall cooling, respectively. The solid lines are the correct results.

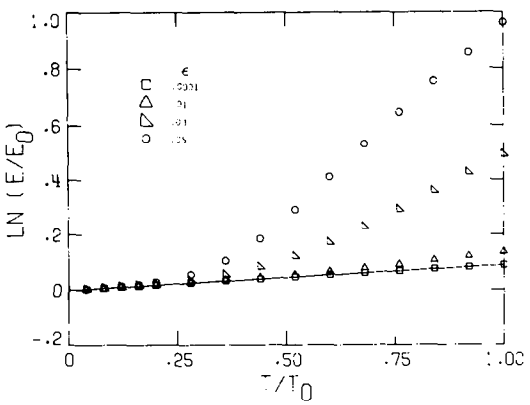

FIG. 14. Computed perturbation energy for a water boundary layer ($\alpha^{-1} = 10{,}000$, $\theta_w/\theta_\infty = 1.1$). The [redacted] were computed by using an 8-point grid in x and a 33-point grid in y ($\varepsilon = 0.0001$ (·), 0.01 (△), 0.03 (◺), 0.05 (○)). The solid line is the linear result.

good agreement with the theory. The calculated energy ratios and errors are given in Table VIII.

In Fig. 13, a strong stabilization effect may be noted when the wall-to-freestream temperature ratio θ_w/θ_∞ is increased from 1 to 1.1 These calculations were performed with $\varepsilon = 0.0001$ using four Fourier spectral modes in the streamwise direction. In order to study the effect of nonlinearity, we have recomputed the $\theta_w/\theta_\infty = 1.1$ case using eight Fourier spectral modes in the streamwise direction for $\varepsilon = 0.0001$, 0.01, 0.03, 0.05. The results are presented in Fig. 14 along with the linear Orr–Sommerfeld solution. It can be seen that the energy rate increases with increasing perturbation amplitude ε. A thorough set of 2-dimensional and 3-dimensional finite amplitude results, produced by the latter two authors in collaboration with D. Bushnell, will be presented elsewhere.

6. Concluding Remarks

A Fourier–Chebyshev spectral method for the solution of the incompressible Navier–Stokes equations has been presented. This fully spectral method is applicable to both the internal and external boundary layers with variable viscosity. The method uses Chebyshev polynomials in the vertical direction and Fourier spectral collocation in the horizontal direction. The continuity and momentum equations are solved as a set of coupled equations without splitting. A staggered grid is employed in the vertical direction so that no numerical pressure boundary conditions are needed. The resulting implicit equations are solved by a preconditioned iterative technique. The algorithm has been subjected to extensive testing by applying it to problems in hydrodynamic stability in channel flow and external

boundary layers with constant and variable viscosity. The results obtained with 33 Chebyshev polynomials are found to be more accurate and require less CPU time than when 257 finite difference grid points are used.

REFERENCES

1. S. A. ORSZAG AND L. C. KELLS, *J. Fluid Mech.* **96** (1980), 159.
2. P. MOIN AND J. KIM, *J. Comput. Phys.* **35** (1980), 381.
3. L. KLEISER AND U. SCHUMANN, Spectral simulation of the laminar–turbulent transition process in plane Poiseuille flow, *in* "Proc. of ICASE Sympos. on Spectral Methods" (R. Voigt, Ed.), SIAM-CBMS, 1983.
4. R. D. MOSER, P. MOIN, AND A. LEONARD, *J. Comput. Phys.* **52** (1983), 524.
5. S. A. ORSZAG AND A. T. PATERA, *J. Fluid Mech.* **128** (1983), 347.
6. P. MARCUS, *J. Fluid. Mech.* **146** (1984), 45.
7. P. MOIN AND J. KIM, *J. Fluid Mech.* **118** (1982), 341.
8. A. WRAY AND M. Y. HUSSAINI, *Proc. R. Soc. London, A* **392** (1984), 373.
9. D. GOTTLIEB, AND S. A. ORSZAG, "Numerical Analysis of Spectral Methods: Theory and Applications," CBMS-NSF Regional Conference Series in Applied Mathematics, SIAM, 1977.
10. M. Y. HUSSAINI, M. D. SALAS, AND T. A. ZANG, in "Advances in Computational Transonics" (W. G. Habashi, Ed.), Pineridge, Swansea, U.K., 1983.
11. S. A. ORSZAG, *J. Comput. Phys.* **37** (1980), 70.
12. R. L. SANI, P. M. GRESHO, R. L. LEE, AND D. F. GRIFFITHS, *Int. J. Numer. Meth. Fluids*, **1** (1981), 17.
13. S. HUBERSON AND Y. MORCHOISNE, "Large Eddy Simulation by Spectral Method or by Multilevel Particle Method," AIAA Paper 83-1880, 1983.
14. T. A. MANTEUFFEL, *Numer. Math.* **28** (1977), 307.
15. S. C. EISENSTAT, H. C. ELMAN, AND M. H. SCHULTZ, SIAM *J. Numer. Anal.* **20** (1983), 345.
16. H. FASEL, *J. Fluid Mech.* **78** (1976), 355.
17. R. L. LOWELL AND E. RESHOTKO, Case Western Reserve University FT AS/TR-73-93, 1974.
18. A. R. WAZZAN, T. OKAMURA, AND A. M. O. SMITH, *J. Heat Transfer* **90** (1968), 109.